The Astrophysical Journal Letters, 970:L39 (8pp), 2024 August 1 https://doi.org/10.3847/2041-8213/ad6316

Discovery of a Barium Blue Straggler Star in M67 and "Sighting" of Its White Dwarf Companion*

Harshit Pal[1,2], Annapurni Subramaniam[1], Arumalla B. S. Reddy[1], and Vikrant V. Jadhav[3]
[1] Indian Institute of Astrophysics, Koramangala II Block, Bangalore, 560034, India
[2] Indian Institute of Science Education and Research, Berhampur, Odisha, 760010, India
[3] Helmholtz-Institut für Strahlen- und Kernphysik, Universität Bonn, Nussallee 14-16, D-53115 Bonn, Germany
Received 2024 May 24; revised 2024 July 1; accepted 2024 July 8; published 2024 July 30

Abstract

We report the discovery of a barium blue straggler star (BSS) in M67, exhibiting enhancements in slow neutron-capture (*s*-)process elements. Spectroscopic analysis of two BSSs (WOCS 9005 & WOCS 1020) and four stars located near the main-sequence turn-off using GALAH spectra, showed that WOCS 9005 has a significantly high abundance of the *s*-process elements ([Ba/Fe] = 0.75 ± 0.08, [Y/Fe] = 1.09 ± 0.07, and [La/Fe] = 0.65 ± 0.06). The BSS (WOCS 9005) is a spectroscopic binary with a known period, eccentricity, and a suspected white dwarf (WD) companion with a kinematic mass of 0.5 $M_{\odot}$. The first "sighting" of the WD in this barium BSS is achieved through multiwavelength spectral energy distribution (SED) with the crucial far-UV data from the UVIT/AstroSat. The parameters of the hot and cool companions are derived using binary fits of the SED using two combinations of models, yielding a WD with $T_{\rm eff}$ in the range 9750–15,250 K. Considering the kinematic mass limit, the cooling age of the WD is estimated as ∼60 Myr. The observed enhancements are attributed to a mass transfer (MT) from a companion asymptotic giant branch star, now a WD. We estimate the accreted mass to be 0.15 $M_{\odot}$, through wind accretion, which increased the envelope mass from 0.45 $M_{\odot}$. The detection of chemical enhancement, as well as the sighting of WD in this system, have been possible due to the recent MT in this binary, as suggested by the young WD.

Unified Astronomy Thesaurus concepts: Open star clusters (1160); Barium stars (135); Blue straggler stars (168); White dwarf stars (1799); S-process (1419); Spectroscopic binary stars (1557); Spectral energy distribution (2129)

1. Introduction

Star clusters are test beds to understand single and binary star evolution. Clusters host a good fraction of binaries (Jadhav et al. 2021) as well as binary products due to evolution and stellar encounters. Among the binaries, the post-mass-transfer (MT) binary systems play an important role in the formation of Type Ia supernovae, blue straggler stars (BSSs), subdwarfs, and extremely low-mass (ELM) white dwarfs (WDs).

The chemical enhancement in the secondary companion due to MT from an evolved primary in a binary has been a topic of research and in particular, the transfer of *s*-process elements synthesized during the thermally pulsing phase of the asymptotic giant branch (AGB) companion (Busso et al. 1999). Even though binaries are plentiful in clusters, only a handful of chemically enriched post-MT binaries have been found (Martins et al. 2017; Van der Swaelmen et al. 2017; Li et al. 2022). The BSSs are likely to be formed via MT (McCrea 1964) or mergers (Andronov et al. 2006), and those formed through an MT in which the primary evolved through an AGB phase (Case C MT; Chen & Han 2008) are potential targets for chemically enriched systems. There is one confirmed barium star (a giant) known in NGC 2420 (Van der Swaelmen et al. 2017), and its orbital properties confirm the presence of an unseen WD. The cluster NGC 5822 has two *s*-process enhanced giants (Santrich et al. 2013). The cluster NGC 6819 has a double-lined spectroscopic binary BSS with barium enhancement and four barium-enhanced BSSs with no radial velocity variations (Milliman et al. 2015). Mathys (1991) detected two Ba-enriched BSSs in M67 (S968 and S1263), which are found to be single members (Geller et al. 2015). This is indeed puzzling as there are many BSSs that are single-lined spectroscopic binaries (SB1s) with unseen WD binaries and should have gone through a Case C MT with detectable chemical enrichment.

In the Galactic field, barium and other *s*-process elements are found to be enhanced in barium (Ba II) stars (McClure 1984). These stars are widely studied (Liu et al. 2009), where many are giants (giant barium stars; Jorissen et al. 2019) and a few are in the main sequence (MS; dwarf barium stars; Escorza et al. 2019). Since McClure et al. (1980) and McClure (1984) showed that Ba II stars are in binaries, it is widely accepted that their enhanced elements came from a companion AGB star, which is now an optically invisible/unseen WD. Therefore, there is a sharp contrast as only a few enhanced systems are seen in the BSSs in star clusters that are formed via the MT process.

Gray et al. (2011) found that barium stars have a real far-UV excess based on the analysis of six barium dwarfs and F-type dwarfs. Secondary stars of a few planetary nebulae have been found to be barium-enhanced, and many studies have characterized the WD in these systems using UV data (Miszalski et al. 2012; Siegel et al. 2012; Miszalski et al. 2013; Merle et al. 2016).

Messier67 (M67; NGC 2682), an old and rich open cluster with solar-like age and metallicity (Hobbs & Thorburn 1991), is a goldmine for studying stellar evolution, stellar dynamics, and binary products. Most notably, this cluster houses a large number of BSSs (Liu et al. 2008; Jadhav & Subramaniam 2021) and the radial velocity surveys have shown a much higher binary fraction among BSSs, 60 ± 24% (Latham 2007;

* This is paper XV of the UVIT Open Cluster Study (UOCS).

Geller et al. 2008). There have been attempts to search for chemical enhancements among the BSSs of M67 (Mathys 1991; Bertelli Motta et al. 2018; Brady et al. 2023). With the help of UV photometric data, several studies reported the detection of ELM WD companions to some of the BSSs (Jadhav et al. 2019; Sindhu et al. 2019; Pandey et al. 2021). Radial velocity monitoring studies of M67 have been extensively carried out under the WIYN open cluster study (WOCS) program, and the orbital parameters of a large number of stars are presented in Geller et al. (2015) and Geller et al. (2021).

WOCS 9005 is a BSS that is an SB1 but located close to the main-sequence turn-off (MSTO; Geller et al. 2015). Jadhav et al. (2019) detected this star in one filter in the far-ultraviolet (FUV) and found a possible hot companion, but mentioned that further observations are needed to confirm the presence of the hot companion. Leiner et al. (2019) estimated a probable rotation of 4.5 days, estimated the unseen WD mass to be $\sim$0.5 $M_{\odot}$, and estimated a gyro-age of $\sim$500 Myr. Geller et al. (2021) published the orbital parameters as well as radial velocity curves.

Here, we present the discovery of WOCS 9005 as a barium BSS with *s*-process enhancement based on *s*-process elemental abundances from GALAH spectra (Buder et al. 2021). We also present the first "sighting" of the WD in the form of excess far-UV flux and estimate the WD parameters from the fits to its spectral energy distribution (SED). This work has many implications, such as the confirmation of the MT process by "seeing the unseen WD" in a barium BSS, the binary MT process at work in the cluster environment, and the physics of accretion processes through stellar wind accretion in a binary system.

2. Data Sets

We have used the Ultra-Violet Imaging Telescope (UVIT) onboard AstroSat catalog of M67 from Jadhav et al. (2021b), with magnitudes along with their errors in the three FUV filters, F148W, F154W, and F169M. We further utilized preexisting photometric data from Swift UVOT Open Clusters Catalog[4] M67 in three UV filters (UVW1, UVM2, and UVW2), and in one optical filter (U; Siegel et al. 2019), and additional archival data (Section 5).

We have used the radial velocity time series data and the orbital parameters from Geller et al. (2021). GALAH is an optical spectroscopic survey that utilizes the HERMES spectrograph ($R = 28{,}000$) at the Anglo-Australian Telescope, offering 678,423 spectra for 588,571 stars, primarily within 2 kpc. We have used the abundance data for M67 stars as well as the spectroscopic data from the GALAH survey.

3. Selection of the Target Based on Abundances from GALAH

Numerous heavy elements were detected in the star by the GALAH survey (Buder et al. 2021), including yttrium (Y), which is part of the first *s*-process peak, as well as barium (Ba) and lanthanum (La), which belong to the second *s*-process peak. We selected stars that (1) are detected in the UVIT images with a good SNR, (2) have a membership from Geller et al. (2021), and (3) have [Ba/Fe] and [Y/Fe] abundance estimates from GALAH. Figures 1(a)–(b) show the [Ba/Fe] and [Y/Fe] abundances against the [Fe/H] values of 88 stars that satisfy all of the above three conditions. Among these 88 stars, 22 have orbital parameters information in the Geller et al. (2021) catalog.

From Figure 1(a), we find that a few stars have an overabundance of barium with respect to the majority of stars.

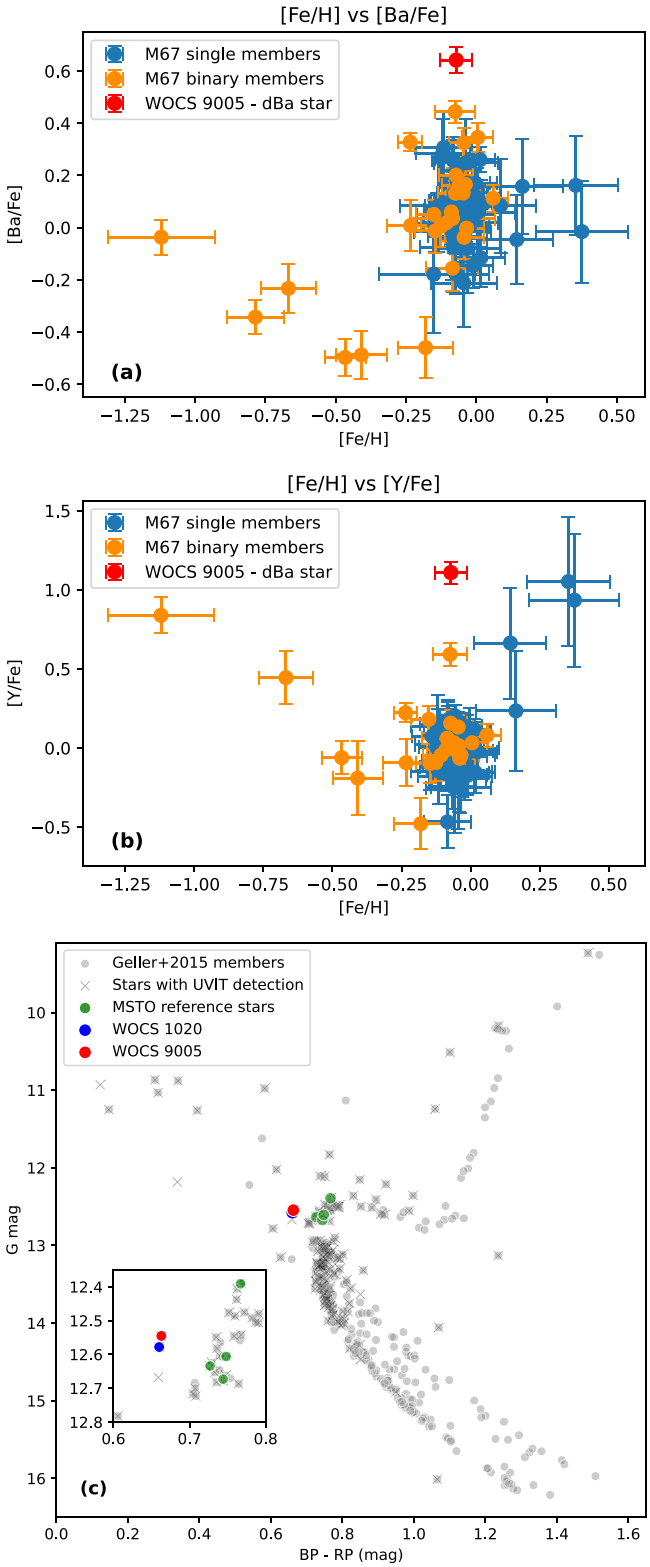

Figure 1. (a) Barium and (b) yttrium abundances of single members (SM) and binary members (BM) of M67 (from Geller et al. 2021) as estimated by GALAH (Buder et al. 2021) are shown. Panel (c) shows the color–magnitude diagram of M67 using the Gaia DR3 data.

[4] https://archive.stsci.edu/hlsp/uvot-oc

Among these, WOCS 9005 is an SB1 and a BSS, which shows high barium abundance. As shown in panel (b), the same star also has high yttrium abundance and stands out with statistically significant excess in comparison to the majority of stars. Therefore, WOCS 9005 is a very strong candidate for a dwarf barium star. It has also been classified as a BSS, and we confirm the classification based on its location as shown in the Gaia color–magnitude diagram (CMD) in Figure 1(c). This star therefore gains importance as a candidate to detect *s*-process chemical enhancement in a BSS, that is likely to be formed via MT.

4. Stellar Parameters and Chemical Composition of WOCS 9005

This section presents independent chemical abundance estimates of the GALAH optical spectra of WOCS 9005, and compares them with those of a similar BSS (WOCS 1020) and four stars located on the MSTO of the cluster (WOCS 4021, 5009, 4004, and 7010, marked in panel (c) of Figure 1). The chemical composition of these MSTO stars is assumed to be representative of the mean cluster abundance. The reduced one-dimensional spectra of the above stars in M67, observed at a spectral resolution of 28,000 are retrieved from the GALAH DR3 Spectral Library.[5] The typical SNR of the spectra is higher than 100 over the wavelength range covered by the high-resolution multifiber spectrograph, HERMES.

A differential abundance analysis relative to the Sun was performed by running the *abfind* driver of MOOG (Sneden 1973) adopting the ATLAS9 one-dimensional, line-blanketed, plane-parallel local thermodynamic equilibrium (LTE) model photospheres computed with updated opacity distribution functions (Castelli & Kurucz 2003) and the measured iron line equivalent widths (EWs) from the observed spectra following the standard LTE abundance analysis technique described in Reddy & Lambert (2019). The stellar parameters (effective temperature ($T_{\rm eff}$), surface gravity ($\log g$), microturbulence velocity (ξ_t) and metallicity ([Fe/H])) were derived by force-fitting the model-generated iron line EWs to the observed ones by imposing the excitation and ionization equilibrium and the requirement that the derived iron line abundances are independent of measured line EWs.

The abundances for Na and the *s*-process elements were derived by fitting synthetic profiles to the observed lines of Na (5688 Å), Y II (4884 and 5729 Å), Ba II (5854 and 6497 Å), and La II (4804 and 5806 Å), following the standard synthetic profile fitting procedure (Reddy & Lambert 2019) where the computed synthetic profiles were smoothed before matching the observed spectra with Gaussian profiles representing the instrumental and rotational ($v \sin i$) broadening of the spectral lines. The line list employed for the spectrum synthesis of Ba II lines includes hyperfine structure components and isotopic shifts (McWilliam 1998), and the fractional contribution of each isotope to solar system Ba abundances (Lodders 2003). Excluding Ti, Cr, Y II (5729 Å), and two La II lines, the spectral lines used for chemical composition analysis are stronger than 10 mÅ, while the former set of lines have EW < 10 mÅ and their measured abundances are sensitive to spectral noise and continuum placement. However, all the key lines of interest (Na, Y, Ba, and La) in the *s*-process-enhanced star WOCS 9005 are stronger than 10 mÅ to derive the best estimates of elemental abundances.

The final stellar parameters and derived abundances along with typical 1σ errors for WOCS 9005 and the comparison star WOCS 1020 selected based on the similarity of stellar parameters with WOCS 9005 are provided in Table 1. The 1σ error is estimated by adding in quadrature the sum of the errors introduced by uncertainties in stellar parmeters and spectrum synthesis/EW analysis. Average [X/Fe] values for four turn-off stars and WOCS 1020 are also presented in the Table 1. The individual abundances and stellar parameters of the four MSTO stars are provided in Table 2.

Entries in Table 1 offer the striking evidence that WOCS 9005 is enhanced with Na and *s*-process elemental abundances relative to MSTO stars including WOCS 1020 (i.e., within the run from Na to La, [X/Fe] ratios for WOCS 1020 and MSTO stars are nearly solar (Table 2), whereas sodium and the *s*-process elements (only) are overabundant in WOCS 9005 over the comparison sample with closely matched [X/Fe] values for all other elements). These results agree well within ± 0.1 dex for almost all elements in common with the abundances reported from the GALAH survey. Figure 2 offers a direct comparison of observed spectra of WOCS 9005 with WOCS 1020 covering the spectral lines due to Na, and *s*-process elements Y, Ba, and La. The line strengths for the *s*-process elements Y, Ba, and La in WOCS 9005 are more pronounced, signifying the reliability of derived overabundances for WOCS 9005.

The presence of sodium (generally observed in stars evolved to red giant branch/AGB phase) along with the *s*-process enrichment, binarity of WOCS 9005, and its current location near the main-sequence turn-off precludes the possibility of formation of WOCS 9005 from the parent cluster gas cloud already enriched with Na and *s*-process elements and indicate the presence of accreted material in the photosphere of WOCS 9005 from its evolved binary companion, which is now a WD. Leiner et al. (2019) derived a kinematic mass of $\sim 0.5\,M_{\odot}$ for the WD companion of WOCS 9005 from the relation connecting the binary mass function $f(m)$ with the radial velocity semiamplitude, orbital period, and eccentricity. The mass of WOCS 9005 was adopted by fitting theoretical PARSEC stellar evolutionary tracks (Bressan et al. 2012) to its position in the CMD. The orbital parameters adopted by Leiner et al. (2019) for the WOCS 9005 binary system are the same as those presented in Geller et al. (2021) via extensive radial velocity observations of M67 members. The orbital parameters and mass estimates of the binary system (WOCS 9005 and its WD companion) are presented in Table 1.

5. "Sighting" of WD in WOCS 9005 from SED

An excess UV flux can indicate the presence of a hot companion star in a binary system, and an SED analysis can detect (1) the presence of FUV excess and (2) fit a double component SED to characterize the hotter and cooler binary companions, as shown in many recent studies (Subramaniam et al. 2018; Jadhav et al. 2019; Sindhu et al. 2019; Panthi et al. 2022, 2023). Following the technique used by Jadhav et al. (2021a), we constructed the SED of the source. UVIT data are merged with observations from longer wavelengths using VOSA's Virtual observatory (Bayo et al. 2008), to build a multiwavelength SED. We obtained photometric fluxes in the range from UV to IR, which include data from UVOT (UVW1, UVM2, UVW2, and U; Siegel et al. 2019), Galaxy Evolution Explorer (GALEX)–GR6 + 7 (near ultraviolet; Martin et al. 2005), Hubble Space Telescope (HST; F140LP, F150LP, and F165LP; Nine et al. 2023), APASS 9 (*B*, *V*, *g*, *r*, *i*; Henden & Munari 2014), Gaia DR3 (G, Gbp, Grp, and Grvs; Vallenari et al. 2023), Pan Starrs PS1 DR2 (*g*, *r*, *i*, *z*, *y*; Chambers et al. 2016), Sloan Digital Sky Survey

[5] https://www.galah-survey.org/dr3/the_spectra/

Table 1
Elemental Abundances and Stellar Parameters for WOCS 9005 and WOCS 1020 and the Average [X/Fe] Values for Four Turn-off Stars and WOCS 1020

Parameter	WOCS 9005	WOCS 1020	Average_TO
[Na I/Fe]	$+0.28 \pm 0.05(1)$	$0.00 \pm 0.05(1)$	$+0.08 \pm 0.07$
[Mg I/Fe]	$+0.07 \pm 0.04(1)$	$+0.03 \pm 0.05(2)$	$+0.05 \pm 0.06$
[Al I/Fe]	$+0.07 \pm 0.05(4)$	$+0.09 \pm 0.03(3)$	$+0.08 \pm 0.02$
[Si I/Fe]	$-0.04 \pm 0.04(4)$	$-0.02 \pm 0.02(3)$	0.00 ± 0.06
[Ca I/Fe]	$-0.01 \pm 0.06(4)$	$-0.01 \pm 0.05(3)$	$+0.03 \pm 0.02$
[Ti I/Fe]	$-0.01 \pm 0.05(3)$	$+0.02 \pm 0.04(2)$	0.00 ± 0.03
[Cr I/Fe]	$-0.05 \pm 0.03(1)$	$-0.02 \pm 0.03(1)$	-0.02 ± 0.03
[Fe I/H]	$-0.10 \pm 0.05(21)$	$-0.11 \pm 0.06(18)$	-0.14 ± 0.02
[Fe II/H]	$-0.11 \pm 0.07(3)$	$-0.09 \pm 0.07(2)$	-0.14 ± 0.02
[Ni I/Fe]	$-0.04 \pm 0.05(9)$	$0.00 \pm 0.05(7)$	0.00 ± 0.04
[Y II/Fe]	$+1.09 \pm 0.07(2)$	$+0.05 \pm 0.08(2)$	$+0.08 \pm 0.02$
[Ba II/Fe]	$+0.75 \pm 0.08(2)$	$+0.12 \pm 0.09(2)$	$+0.14 \pm 0.04$
[La II/Fe]	$+0.65 \pm 0.06(2)$	$+0.09 \pm 0.06(2)$	$+0.05 \pm 0.07$
$T_{\rm eff}$ (K)[a]	6350 ± 50	6350 ± 50	...
log g (cm s^{-2})[a]	4.2 ± 0.2	4.2 ± 0.2	...
ξ_t (km s^{-1})[a]	1.47 ± 0.1	1.70 ± 0.1	...
[Fe/H] (dex)[a]	-0.10 ± 0.05	-0.11 ± 0.06	...
$v \sin i$ (km s^{-1})[a]	15.0 ± 2.0	14.0 ± 2.0	...
M $(M_\odot)$[b]	1.37 ± 0.04	1.30 ± 0.05	...
R $(R_\odot)$[b]	1.99 ± 0.06	1.80 ± 0.05	...

RV_{COM} (km s^{-1})	Period (days)	RV_{semi} (km s^{-1})	e	$f(m)$ $(10^{-2} M_\odot)$	$a \sin i$ $(10^{11}$ $m)$	M_1 $(M_\odot)$	M_{WD} $(M_\odot)$
32.91 ± 0.16	2769 ± 18	5.1 ± 0.3	0.15 ± 0.05	3.7 ± 0.6	1.92 ± 0.11	1.37 ± 0.04	0.5

Component	$T_{\rm eff}$ (K)	$R(R_\odot)$	$L(L_\odot)$	log g	χ^2_r	vgf^2_b
		Kurucz + Koester				
WOCS 9005A	6500^{+250}_{-250}	$1.85^{+0.03}_{-0.03}$	$5.52^{+1.15}_{-1.15}$	$3.5^{+0.5}_{-0.5}$	14.2	0.25
WOCS 9005B (Best fit)	$11,000^{+250}_{-250}$	$0.063^{+0.001}_{-0.001}$	$0.0525^{+0.0014}_{-0.0014}$	$9.50^{+0.00}_{-0.25}$	14.28	0.28
WOCS 9005B (Top 1 percentile)	9000–12,000	0.036–0.138	0.025–0.113	6.5–9.5	<30.94	<21.5
		Kurucz_UVBLUE + Koester				
WOCS 9005A	6500^{+500}_{-500}	$1.85^{+0.03}_{-0.03}$	$5.52^{+1.15}_{-1.15}$	$3.5^{+0.5}_{-0.5}$	14.1	0.17
WOCS 9005B (Best fit)	$12,500^{+250}_{-250}$	$0.0221^{+0.0022}_{-0.0004}$	$0.0108^{+0.0011}_{-0.0003}$	$9.50^{+0.00}_{-0.25}$	28.03	0.55
WOCS 9005B (Top 1 percentile)	9750–15,250	0.009–0.056	0.004–0.025	6.5–9.5	<29.86	<19.9

Note. The numbers in the parentheses are the number of lines employed for the abundance measurement of an element. The estimated parameters of WOCS 9005 and WOCS 1020 using spectroscopy and photometry are shown below, followed by orbital parameters and mass of the components of WOCS 9005 (Leiner et al. 2019; Geller et al. 2021) and estimated parameters of the cooler and hotter companions from the SED fits. RV_{COM} = center-of-mass radial velocity of binary, RV_{semi} = radial velocity semiamplitude, e = orbital eccentricity, $a \sin i$ = projected semimajor axis, $f(m) = (M_2 \sin i)^3/(M_1 + M_2)^2$.
[a] Estimated through spectral analysis.
[b] Obtained via PARAM, a web interface for the Bayesian estimation of stellar parameters (http://stev.oapd.inaf.it/cgi-bin/param_1.3).

DR12 (u, g, r, i, z), Two Micron All Sky Survey All-Sky Point Source Catalog (J, H, Ks; Cohen et al. 2006), and Wide-field Infrared Survey Explorer (W1, W2, W3, and W4; Wright et al. 2010). The fluxes are extinction (reddening) corrected based on the established extinction–wavelength relations given by Fitzpatrick (1999) and Indebetouw et al. (2005). We have adopted a distance modulus of 9.6 ± 0.04 mag, solar metallicity, and reddening $E(B-V) = 0.041 \pm 0.004$ mag (Taylor 2006).

To estimate the parameters of WOCS 9005, we first fitted the optically bright component (A) with two models using the BINARY SED FITTING Python code (Jadhav et al. 2021a), which is based on χ^2 minimization technique, (i) Kurucz model (Castelli & Kurucz 2003) and (ii) a hybrid Kurucz_UVBLUE model, which uses UVBLUE model spectra (Rodríguez-Merino et al. 2005) within the 580–4700 Å range and Kurucz spectra outside the wavelength range. Both models were fitted using the parameter range as follows: log $g = 3$–5, $T_{\rm eff} = 3500$–10,000 K, and [Fe/H] = 0 dex. Both models fitted the A component with similar parameters and the residual flux showed a significant UV excess as indicated by high fractional residuals (>50%), pointing to the "sighting" of the WD. Due to the substantial UV excess, we performed a double-component fit for both cases. We used the Koester model (Koester 2010) to fit the hotter component (B), within a temperature range of 5000–80,000 K and log g range of 6.5–9.5.

The results of the binary SED fit are shown in Figure 3 and are tabulated in Table 1. The $T_{\rm eff}$, radius, and the log g estimates of the cooler component are in excellent agreement with the spectroscopic estimates. We are able to "sight" and characterize the hot companion of WOCS 9005 for the first time. The Kurucz and Kurucz_UVBLUE model binary SEDs result in different parameters of the hotter component. The χ^2 and fractional residual in Kurucz fitting is better compared to the Kurucz_UVBLUE model. Overall, the hot companion

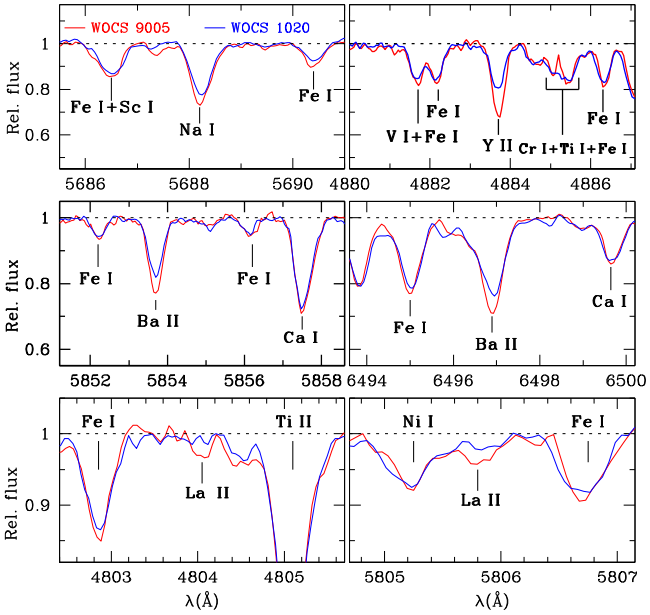

Figure 2. Observed spectra of WOCS 9005 (red) and WOCS 1020 (blue) covering the wavelength regions containing Na and the *s*-process elements Y, Ba, and La. The spectral lines due to other species are also shown.

resembles a WD with $T_{\rm eff}$ in the range of 11,000–12,500 K, with a radius of ∼0.02–0.06 $R_{\odot}$, and with a log g of ∼9.5. The parameters of the cooler component estimated using an SED-fitting technique by Nine et al. (2023, as reported in their Table 1), match well with our estimations. They did not detect UV excess for WOCS 9005 based on the (F150N−F165LP, and F150N) CMD, where the derived HST FUV narrowband magnitude and color were compared with UVBLUE model-based synthetic photometry. We used the same HST photometry in the observed bands and detected noticeable excess UV flux ($\Delta F/F = 0.30$, 0.36, and 0.41 for F165LP, F150LP, and F140LP, respectively) when compared to the UVBLUE model prediction (middle panel of Figure 3). The discrepancy in identifying the UV excess in the source may be due to the different techniques (CMD versus SED) used to identify the excess and their usage of the derived narrowbands.

The photometric mass was estimated by comparing the position of the hotter companion in the H–R diagram with WD models (Holberg & Bergeron 2006; Althaus et al. 2013). The estimated mass of the companion WD is ∼0.176–0.3 $M_{\odot}$ and the log(age) ∼7.5 (for 0.3 $M_{\odot}$)–9 (for 0.176 $M_{\odot}$), based on the best-fitted SED models. However, if we consider the top 1 percentile result of the χ^2 fits, we obtain a wider range of WD parameters, resulting in a temperature range of 9750–15,250 K, mass range of 0.17–0.9 $M_{\odot}$, and log(age) range of 6.1–9. The kinematic mass of 0.5 $M_{\odot}$ falls within the above range and has a corresponding cooling age of ∼60 Myr for the parameter range of the Kurucz_UVBLUE model fit. We therefore conclude that the SED analysis has indeed "sighted" the WD and characterized the hot companion. The WD cooling curves presented above assume that the WD has reached equilibrium and no more fusion is happening. However, as shown by Althaus et al. (2013, Figure 4), occasional flashes change the photometric parameters of the WDs. Thus, the above WD mass estimations depend on the evolutionary stage of the WD, and the unavailability of such information contributes to the uncertainty in the photometric mass estimation. However, including both binary fits, it is found to be a young system that has experienced a recent MT. Though the photometric mass may be less reliable, the youth of the system is confirmed.

6. Modeling (WOCS 9005): A Dwarf Barium Star

MT in Ba II stars from AGB companions predominantly occurs through stellar wind accretion rather than Roche lobe overflow (Boffin & Jorissen 1988). Subsequent researchers have employed similar methods to develop both qualitative and quantitative models of the MT scenario in Ba II stars (Cui et al. 2008; Husti et al. 2009; Stancliffe 2021). In this section, we present the formation and evolution scenario of WOCS 9005 through MT from an AGB star by adopting the wind accretion model of Boffin & Jorissen (1988).

WOCS 9005 has a metallicity of $[{\rm Fe/H}] = -0.10 \pm 0.05$, suggesting that it likely had a solar-scaled abundance for each element before accretion. Therefore, the initial abundance of *s*-process elements should be $[{\rm Ba/Fe}]_{\rm initial} = 0$, $[{\rm Y/Fe}]_{\rm initial} = 0$, and $[{\rm La/Fe}]_{\rm initial} = 0$. After accretion, the observed abundances were $[{\rm Ba/Fe}] = 0.75 \pm 0.08$, $[{\rm Y/Fe}] = 1.09 \pm 0.07$, and $[{\rm La/Fe}] = 0.65 \pm 0.06$. Since the accreted matter is heavier than the initial envelope composition of the MS star, thermohaline mixing occurs, diluting the accreted matter into the entire envelope (for a detailed explanation, see Stancliffe & Jeffery 2007). The initial envelope mass of approximately 3 times the mass transferred by the AGB ($M^{T}_{\rm AGB}$; containing all the heavy metal) is derived for the accreting star using the formula given in Equation (1) of Husti et al. (2009). The present-day semimajor axis (A) based on the orbital parameters is 7.12×10^{11} m. Although the semimajor axis can change following MT in the binary system, as suggested by Boffin & Jorissen (1988) and Husti et al. (2009), treating a constant value of A is a reasonable assumption during the superwind phase experienced at the end of the AGB phase. Based on these assumptions, the accreted mass calculated for a stellar wind velocity ($V_{\rm wind}$) of 30 km s^{-1} using the MT formula given in Equation (6) of Boffin & Jorissen (1988) & Equation (4) of Husti et al. (2009) is approximately 0.15 $M_{\odot}$. The above value of $V_{\rm wind}$ is consistent with the mean of the $V_{\rm wind}$ in the range 20–40 km s^{-1} estimated for the AGB stars (Pottasch 1984; Knapp 1985). Consequently, based on the earlier relationship, the initial mass of the MS (now a barium dwarf) star's envelope was ≈0.45 $M_{\odot}$ and the final envelope mass after MT is ≈0.6 $M_{\odot}$. This analysis serves as our attempt to model the WOCS 9005 binary system using the method of Boffin & Jorissen (1988), where the barium dwarf would have formed via MT through the stellar wind from AGB donor to MS star. However, an in-depth analysis of the WOCS 9005 binary system in the future would offer greater insight into its characteristics, evolution, and MT mechanism.

7. Discussion and Conclusion

There are several searches and characterizations of dwarf barium stars using high-resolution spectroscopic data (Mardini et al. 2024; Roriz et al. 2024). There are a very small number of known dwarf barium stars (Roriz et al. 2024). The $T_{\rm eff}$ and the log g range of the WOCS 9005 fall in the range of these parameters of dwarf barium stars studied by Roriz et al. (2024). WOCS 9005 has relatively lower abundances of Ba and Y in comparison to those in the three stars analyzed by Roriz et al. (2024). The Y and La abundances of WOCS 9005 are very similar to those in the giant barium star,

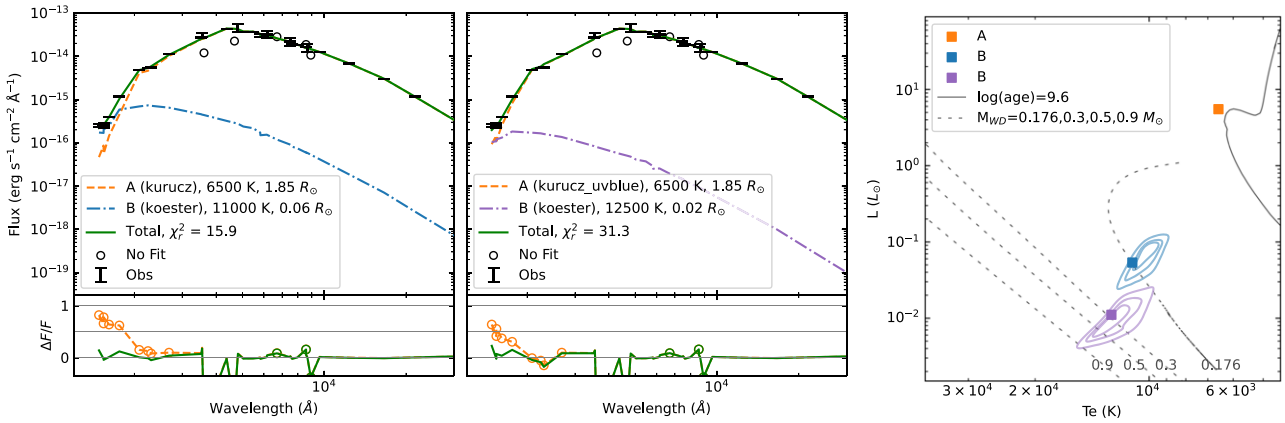

Figure 3. Binary SEDs of WOCS 9005. The left panel shows the binary fit using Kurucz and Koester models. The middle panel shows the binary fit using Kurucz_UVBLUE and Koester models. The fitted SEDs for A component (orange), B component (blue for Kurucz and purple for Kurucz_UVBLUE), and total (green). The bottom subpanel shows the fractional residual flux for the A component and total binary SED. The observed points are shown as black error bars and data removed during fitting is shown as black circles. The right panel shows the H–R diagram of the components based on SED fit parameters, with the same colors as the SEDs. The contours represent the top 1 percentile fits of the corresponding model. The PARSEC isochrone of log(age) 9.6 (gray curve) and WD cooling curves for WD masses of 0.176 (Althaus et al. 2013), 0.3, 0.5, and 0.9 (Holberg & Bergeron 2006) are shown for reference.

NGC 2420-173 ([Y/Fe] = 1.0; [La/Fe] = 0.62; P = 1479 days; e = 0.43; Jorissen et al. 2019), which is found to be slightly metal-poor ([Fe/H] = −0.26; Van der Swaelmen et al. 2017).

Though our derivation of $T_{\rm eff}$ and $\log g$ for WOCS 9005 matches excellently with Nine et al. (2024) values, the barium enhancement of WOCS 9005 was not uncovered by their analysis as they assume a higher value of ξ_t. The estimation of Ba abundance from the line EW/synthesis is sensitive to the assumed value of ξ_t (Reddy & Lambert 2017). We note that their estimated [Ba/Fe] values for WOCS 8012 and 10014 (where they assume a lower value of ξ_t) are similar, whereas that for WOCS 9005 differs by more than 0.6 dex with respect to GALAH survey results.

Escorza et al. (2019) studied a number of field dwarf barium stars and their orbital properties. In their Figure 9, the giant and dwarf barium stars are shown in the period–eccentricity diagram. WOCS 9005, with a period of 2769 ± 18 days and eccentricity 0.15 ± 0.05, falls in the densely populated region of known giant barium stars, though there are no known dwarf barium stars in the region. The orbital parameters of NGC 2420-173 fall within a similar range. Overall, WOCS 9005 fits well with the orbital kinematics of the known barium stars.

This is the first barium BSS star with a photometrically detected hot companion. This is also the first estimate of the WD properties and model-based age of the WD companion of a barium BSS.

WOCS 9005 and WOCS 1020 are both BSSs with very similar properties, though WOCS 1020 is a single member with FUV detection. Though many previous studies considered the above two stars as BSSs, Geller et al. (2015) excluded them in their conservative list of BSSs. On the other hand, Leiner et al. (2019) considered these two as blue lurkers, which are stars on the MS, but have experienced MT as inferred from their fast rotation. Panel (c) of Figure 1, confirms that these stars are indeed BSSs. Among the MSTO comparison stars, WOCS 4021, 5009, and 4004 are SB1s and have estimated orbital properties. Our analysis finds that these three SB1s on the MSTO have very similar abundances, which is also similar to the abundance of the BSS WOCS 1020.

We note that there is no detection of the three reference MSTO SB1s in the UVIT-FUV, even though they have periods in the range 4600–7400 days, indicating that either the companions are much fainter MS stars or relatively older WDs. The detection of overabundance of s-process elements in WOCS 9005 is due to a recent MT, as suggested by the young WD. We note that there are a few more SB1 systems with periods similar to WOCS 9005 in M67 but show a mild barium enhancement, as seen from Figure 1, which we will explore in the future. It is possible that the abundance enhancement is a short-lived phenomenon in BSSs. The timescale for diffusion or gravitational settling to effectively deplete the overabundance from the surface to the lower layers is likely to be faster for MS stars relative to giants due to their higher gravity, though there are no theoretical estimations. Missions such as UVIT/AstroSat and GALEX can only detect hotter and newly formed WDs. More sensitive missions, such as the proposed INSIST mission (Subramaniam 2022), along with its spectroscopic capability, will be able to unearth WDs in many post-MT binary systems, including BSSs and barium stars.

Acknowledgments

We thank the referee for valuable suggestions. A.S. acknowledges support from SERB power fellowship. V.J. thanks the Alexander von Humboldt Foundation for their support. UVIT project is a result of the collaboration between IIA, Bengaluru, IUCAA, Pune, TIFR, Mumbai, several centers of ISRO, and CSA. This publication makes use of VOSA, developed under the Spanish Virtual Observatory project. This work has made use of data from the European Space Agency (ESA) mission Gaia (https://www.cosmos.esa.int/gaia), processed by the Gaia Data Processing and Analysis Consortium (DPAC; https://www.cosmos.esa.int/web/gaia/dpac/consortium).

Facilities: Astrosat(UVIT), Swift(UVOT), Gaia, AAT (HERMES), GALEX, AAVSO(APASS), PS1, Sloan, CTIO:2-MASS, WISE.

Appendix

This section provides the individual elemental abundances and stellar parameters for four turn-off stars (Table 2), which were used to estimate average abundances in Table 1.

Table 2
Elemental Abundances [X/Fe] for Four Turn-off Stars, Which Were Used to Estimate Average Abundances in Table 1

Parameter	WOCS 4021	WOCS 5009	WOCS 4004	WOCS 7010
[Na I/Fe]	$+0.15 \pm 0.05(1)$	$-0.02 \pm 0.05(1)$	$+0.08 \pm 0.05(1)$	$+0.13 \pm 0.05(1)$
[Mg I/Fe]	$+0.12 \pm 0.05(3)$	$+0.10 \pm 0.04(2)$	$-0.02 \pm 0.05(2)$	$+0.01 \pm 0.05(3)$
[Al I/Fe]	$+0.08 \pm 0.03(3)$	$+0.08 \pm 0.02(2)$	$+0.05 \pm 0.05(4)$	$+0.09 \pm 0.04(4)$
[Si I/Fe]	$-0.02 \pm 0.03(3)$	$+0.04 \pm 0.02(4)$	$-0.08 \pm 0.04(4)$	$+0.09 \pm 0.04(4)$
[Ca I/Fe]	$+0.02 \pm 0.04(2)$	$+0.01 \pm 0.05(3)$	$+0.06 \pm 0.04(2)$	$+0.05 \pm 0.06(3)$
[Ti I/Fe]	$-0.02 \pm 0.04(1)$	$+0.01 \pm 0.05(3)$	$-0.04 \pm 0.04(2)$	$+0.05 \pm 0.05(3)$
[Cr I/Fe]	$-0.04 \pm 0.03(1)$	$-0.06 \pm 0.03(1)$	$-0.02 \pm 0.03(1)$	$+0.03 \pm 0.03(1)$
[Fe I/H]	$-0.15 \pm 0.05(20)$	$-0.15 \pm 0.05(21)$	$-0.11 \pm 0.05(21)$	$-0.16 \pm 0.05(20)$
[Fe II/H]	$-0.16 \pm 0.06(2)$	$-0.15 \pm 0.07(2)$	$-0.11 \pm 0.07(2)$	$-0.15 \pm 0.06(2)$
[Ni I/Fe]	$-0.01 \pm 0.06(9)$	$+0.07 \pm 0.06(7)$	$-0.01 \pm 0.05(9)$	$-0.05 \pm 0.06(7)$
[Y II/Fe]	$+0.09 \pm 0.08(2)$	$+0.07 \pm 0.08(2)$	$+0.10 \pm 0.07(2)$	$+0.08 \pm 0.07(2)$
[Ba II/Fe]	$+0.20 \pm 0.09(2)$	$+0.15 \pm 0.09(2)$	$+0.10 \pm 0.09(2)$	$+0.12 \pm 0.09(2)$
[La II/Fe]	$+0.08 \pm 0.07(2)$	$+0.09 \pm 0.07(2)$	$-0.07 \pm 0.06(2)$	$+0.08 \pm 0.06(2)$
$T_{\rm eff}$ (K)[a]	6050 ± 50	5975 ± 50	6000 ± 50	6100 ± 50
$\log g$ (cm s^{-2})[a]	4.0 ± 0.2	3.9 ± 0.2	4.2 ± 0.2	4.0 ± 0.2
ξ_t (km s^{-1})[a]	1.35 ± 0.1	1.24 ± 0.1	1.42 ± 0.1	1.66 ± 0.1
[Fe/H] (dex)[a]	-0.15 ± 0.04	-0.15 ± 0.04	-0.11 ± 0.04	-0.16 ± 0.03
$v \sin i$ (km s^{-1})[a]	10.0 ± 2.0	8.0 ± 2.0	8.0 ± 2.0	9.0 ± 2.0
M $(M_\odot)$[b]	1.23 ± 0.03	1.14 ± 0.02	1.38 ± 0.06	1.23 ± 0.04
R $(R_\odot)$[b]	2.03 ± 0.05	1.83 ± 0.06	2.46 ± 0.14	1.97 ± 0.05

Name	RV_{COM} (km s^{-1})	Period (days)	RV_{semi} (km s^{-1})	e	$f(m)$ ($10^{-2} M_\odot$)	$a \sin i$ (10^{11} m)	M_1 ($M_\odot$)	M_{WD} ($M_\odot$)
WOCS 4021	34.46 ± 0.16	6166 ± 21	7.0 ± 4.0	0.83 ± 0.07	4.0 ± 7.0	3.40 ± 1.90	1.23 ± 0.03	0.49
WOCS 5009	34.33 ± 0.07	4600 ± 110	1.65 ± 0.09	0.21 ± 0.04	0.20 ± 0.03	1.02 ± 0.06	1.14 ± 0.02	0.15
WOCS 4004	34.75 ± 0.19	7400 ± 300	3.1 ± 0.9	0.70 ± 0.14	0.8 ± 0.8	2.2 ± 0.8	1.38 ± 0.63	0.28

Note. The numbers in the parentheses are the number of lines employed for the abundance measurement of an element. The stellar parameters estimated using spectroscopy are shown below, followed by orbital parameters (Geller et al. 2021) and the mass of both components. RV_{COM} = center-of-mass radial velocity of binary, RV_{semi} = radial velocity semiamplitude, e = orbital eccentricity, a sin$i$ = projected semimajor axis, $f(m) = (M_2 \sin i)^3/(M_1 + M_2)^2$.
[a] Obtained through spectral analysis.
[b] Obtained via PARAM.

ORCID iDs

Harshit Pal https://orcid.org/0009-0001-8079-3471
Annapurni Subramaniam https://orcid.org/0000-0003-4612-620X
Arumalla B. S. Reddy https://orcid.org/0000-0003-2754-641X
Vikrant V. Jadhav https://orcid.org/0000-0002-8672-3300

References

Althaus, L. G., Miller Bertolami, M. M., & Córsico, A. H. 2013, A&A, 557, A19
Andronov, N., Pinsonneault, M., & Terndrup, D. 2006, ApJ, 646, 1160
Bayo, A., Rodrigo, C., y Navascués, D. B., et al. 2008, A&A, 492, 277
Bertelli Motta, C., Pasquali, A., Caffau, E., & Grebel, E. K. 2018, MNRAS, 480, 4314
Boffin, H., & Jorissen, A. 1988, A&A, 205, 155
Brady, K., Sneden, C., Pilachowski, C., et al. 2023, AJ, 166, 154
Bressan, A., Marigo, P., Girardi, L., et al. 2012, MNRAS, 427, 127
Buder, S., Sharma, S., Kos, J., et al. 2021, MNRAS, 506, 150
Busso, M., Gallino, R., & Wasserburg, G. J. 1999, ARA&A, 37, 239
Castelli, F., & Kurucz, R. L. 2003, in IAU Symp. 210, Modeling of Stellar Atmospheres, ed. N. Piskunov, W. W. Weiss, & D. F. Gray (San Francisco, CA: ASP), A20
Chambers, K. C., Magnier, E., Metcalfe, N., et al. 2016, arXiv:1612.05560
Chen, X., & Han, Z. 2008, MNRAS, 387, 1416
Cohen, J. G., Hsieh, S., Metchev, S., Djorgovski, S., & Malkan, M. 2006, AJ, 133, 99
Cui, W.-Y., Zhang, B., Quan, Y.-M., Zhou, G.-D., & Chen, Y.-P. 2008, Ap&SS, 314, 351
Escorza, A., Karinkuzhi, D., Jorissen, A., et al. 2019, A&A, 626, A128
Fitzpatrick, E. L. 1999, PASP, 111, 63
Geller, A. M., Latham, D. W., & Mathieu, R. D. 2015, AJ, 150, 97
Geller, A. M., Mathieu, R. D., Harris, H. C., & McClure, R. D. 2008, AJ, 135, 2264
Geller, A. M., Mathieu, R. D., Latham, D. W., et al. 2021, AJ, 161, 190
Gray, R., McGahee, C., Griffin, R., & Corbally, C. 2011, AJ, 141, 160
Henden, A., & Munari, U. 2014, CoSka, 43, 518
Hobbs, L., & Thorburn, J. 1991, AJ, 102, 1070
Holberg, J., & Bergeron, P. 2006, AJ, 132, 1221
Husti, L., Gallino, R., Bisterzo, S., Straniero, O., & Cristallo, S. 2009, PASA, 26, 176
Indebetouw, R., Mathis, J., Babler, B., et al. 2005, ApJ, 619, 931
Jadhav, V. V., Pandey, S., Subramaniam, A., & Sagar, R. 2021a, JApA, 42, 89
Jadhav, V. V., Pennock, C. M., Subramaniam, A., Sagar, R., & Nayak, P. K. 2021b, MNRAS, 503, 236
Jadhav, V. V., Roy, K., Joshi, N., & Subramaniam, A. 2021, AJ, 162, 264
Jadhav, V. V., Sindhu, N., & Subramaniam, A. 2019, ApJ, 886, 13
Jadhav, V. V., & Subramaniam, A. 2021, MNRAS, 507, 1699
Jorissen, A., Boffin, H., Karinkuzhi, D., et al. 2019, A&A, 626, A127
Knapp, G. 1985, ApJ, 293, 273
Koester, D. 2010, MmSAI, 81, 921
Latham, D. W. 2007, HiA, 14, 444
Leiner, E., Mathieu, R. D., Vanderburg, A., Gosnell, N. M., & Smith, J. C. 2019, ApJ, 881, 47
Li, Y., Bedding, T. R., Murphy, S. J., et al. 2022, NatAs, 6, 673
Liu, G., Deng, L., Chávez, M., et al. 2008, MNRAS, 390, 665
Liu, G.-Q., Liang, Y.-C., & Deng, L.-C. 2009, RAA, 9, 431
Lodders, K. 2003, ApJ, 591, 1220
Mardini, M. K., Frebel, A., Betre, L., et al. 2024, MNRAS, 528, 2912
Martin, D. C., Fanson, J., Schiminovich, D., et al. 2005, ApJ, 619, L1
Martins, F., Mahy, L., & Hervé, A. 2017, A&A, 607, A82

Mathys, G. 1991, A&A, 245, 467
McClure, R. D. 1984, PASP, 96, 117
McClure, R. D., Fletcher, J., & Nemec, J. M. 1980, ApJL, 238, L35
McCrea, W. 1964, MNRAS, 128, 147
McWilliam, A. 1998, AJ, 115, 1640
Merle, T., Jorissen, A., Van Eck, S., Masseron, T., & Van Winckel, H. 2016, A&A, 586, A151
Milliman, K. E., Mathieu, R. D., & Schuler, S. C. 2015, AJ, 150, 84
Miszalski, B., Boffin, H. M., Frew, D. J., et al. 2012, MNRAS, 419, 39
Miszalski, B., Boffin, H. M., Jones, D., et al. 2013, MNRAS, 436, 3068
Nine, A. C., Mathieu, R. D., Gosnell, N. M., & Leiner, E. M. 2023, ApJ, 944, 145
Nine, A. C., Mathieu, R. D., Schuler, S. C., & Milliman, K. E. 2024, arXiv:2405.20242
Pandey, S., Subramaniam, A., & Jadhav, V. V. 2021, MNRAS, 507, 2373
Panthi, A., Subramaniam, A., Vaidya, K., et al. 2023, MNRAS, 525, 1311
Panthi, A., Vaidya, K., Jadhav, V., et al. 2022, MNRAS, 516, 5318
Pottasch, S. R. 1984, Planetary nebulae. A study of late stages of stellar evolution, Vol. 107 (Dordrecht: Reidel)
Reddy, A. B. S., & Lambert, D. L. 2017, ApJ, 845, 151
Reddy, A. B. S., & Lambert, D. L. 2019, MNRAS, 485, 3623
Rodríguez-Merino, L. H., Chavez, M., Bertone, E., & Buzzoni, A. 2005, ApJ, 626, 411
Roriz, M., Holanda, N., da Conceição, L., et al. 2024, arXiv:2402.14709
Santrich, O. K., Pereira, C., & De Castro, D. 2013, AJ, 146, 39
Siegel, M. H., Hoversten, E., Bond, H. E., Stark, M., & Breeveld, A. A. 2012, AJ, 144, 65
Siegel, M. H., LaPorte, S. J., Porterfield, B. L., Hagen, L. M. Z., & Gronwall, C. A. 2019, AJ, 158, 35
Sindhu, N., Subramaniam, A., Jadhav, V. V., et al. 2019, ApJ, 882, 43
Sneden, C. A. 1973, PhD thesis, Univ. of Texas, Austin
Stancliffe, R. J. 2021, MNRAS, 505, 5554
Stancliffe, R. J., & Jeffery, C. S. 2007, MNRAS, 375, 1280
Subramaniam, A. 2022, JApA, 43, 80
Subramaniam, A., et al. 2018, MNRAS, 481, 226
Taylor, B. 2006, AJ, 133, 370
Vallenari, A., Brown, A. G., Prusti, T., et al. 2023, A&A, 674, A1
Van der Swaelmen, M., Boffin, H. M., Jorissen, A., & Van Eck, S. 2017, A&A, 597, A68
Wright, E. L., Eisenhardt, P. R., Mainzer, A. K., et al. 2010, AJ, 140, 1868